Scientia Iranica, Vol. 11, No. 4, pp 292–301

SCIENTIA IRANICA

Numerical Study of Detonation Instability for a Two-Step Kinetics Model

K. Mazaheri*, S.A. Hashemi[1] and J.H. Lee[2]

The stability of CJ detonations has been investigated numerically with a two-step kinetics model. The reaction model consists of a non-heat release induction step, followed by an exothermic step. Both steps are governed by the Arrhenius kinetics model. The effect of activation energies associated with these steps on the detonation front behavior has been studied. This study was arranged in two stages. At each stage, one of the activation energies was kept constant and the other one was changed. In the steady detonation structure, the activation energies of the first and second steps (Ea_1, Ea_2) control the induction and reaction lengths, respectively. Increasing Ea_1 (for a fixed Ea_2) increases induction length and destabilizes a detonation, the same behavior as a one-step model. Increasing Ea_2 first increases reaction length and has a stabilizing effect (i.e., the amplitude of oscillation decreases). Further increasing Ea_2 has a destabilizing effect. The present study shows that the ratio of the reaction length to the induction length characterizes general features of detonation stability.

INTRODUCTION

Detonation waves are composed of a lead shock that initiates chemical reaction in the combustible mixture and the release of chemical energy, which sustains the lead shock. In this paper, only self-sustaining detonations that travel about the CJ velocity are studied. Detonations that are supported with pistons and whose velocity is greater than the CJ value, are not considered here. The first theoretical work about detonation was the CJ theory that was proposed by Chapman and Jouguet [1]. They assumed that the thickness of a detonation wave is negligible and the wave travels with a constant velocity. This theory predicts the velocity, pressure and other thermodynamic properties that are in very good agreement with experiments.

The steady, one-dimensional structure of a detonation wave was first determined independently by Zeldovich, Von-Neumann and Doring [1] and is known as the ZND structure.

In practice, a stable one-dimensional detonation wave is seldom observed. Experimental observations show that self-sustaining detonation waves exhibit a significant three-dimensional unsteady structure. However, average velocity is always about the CJ value. According to Strehlow, the unstable structure of detonation waves was observed first by Campbell and Woodhead [2]. Two regimes of detonation instability were observed when blunt-body projectiles were fired into a reactive atmosphere [3,4]. The first involved regular periodic oscillations of the flow field, while the second showed less regular with larger-amplitude oscillations.

The first formal linear stability study of detonation waves was conducted by Erpenbeck [5], who used a Laplace transform approach to study the behavior of small-amplitude disturbances for a plane steady detonation wave. Parameters that were studied by Erpenbeck are heat of combustion, wave number of disturbances and the activation energy of the combustion reaction.

Lee and Stewart [6] developed a normal mode approach to the linear stability problem. They employed a two-point numerical boundary value-shooting algorithm to determine the stability characteristics of detonations. Their study provides highly resolved information about linear stability characteristics, neutral stability boundaries and growth rates of unstable disturbances.

Other works, such as those due to Buckmaster

*. *Corresponding Author, Department of Mechanical Engineering, Tarbiat Modarres University, Tehran, I.R. Iran.*

1. *Department of Mechanical Engineering, Tarbiat Modarres University, Tehran, I.R. Iran.*
2. *Department of Mechanical Engineering, McGill University, Montreal, Canada.*

and Ludford [7], have been handicapped in the physical interpretations of the various modes of instability. Sharpe [8] developed a new normal mode approach and applied it to a detonation with a single one-step reaction. This method was found to be superior to that of previous researchers in the sense that the CJ case was well posed and the effect of much higher activation energies was considered.

Most work on the stability analysis of detonations, have used a one-step, irreversible reaction with an Arrhenius form of the reaction rate. In the one-step Arrhenius type reaction model, the linear stability analysis indicates that increasing the activation energy destabilizes the detonation.

In parallel with linear stability analyses, there have been numerous studies concerned with the numerical simulation of the pulsating detonation instability with Arrhenius one-step reaction kinetics. Utilizing characteristic and finite difference techniques, respectively, Fickett and Wood [9] and Abouseif and Toong [10] were able to reproduce the salient stability features that were predicted by Erpenbeck. Using advanced numerical methods, a significant improvement in the quality and accuracy of numerical simulation was obtained by Bourlioux et al. [11]. Those simulations were able to obtain numerical results in close agreement with the theoretical predictions. In a one-dimensional simulation, the detonation instability appears as the oscillatory behavior of the detonation front. By increasing the activation energy of a one-step model, numerical simulation yields a range of linear oscillation to chaotic oscillatory behavior of the shock front. Stable detonation has a uniform behavior of the shock front and travels with a constant CJ velocity. The structure of a stable detonation obtained from the numerical simulation is identical to the steady ZND structure.

Short and Quirk [12] carried out linear stability analysis and direct numerical simulation of detonation by making use of a three-step chain-branching reaction model. They used the chain-branching crossover temperature as a bifurcation parameter. This parameter controls the ratio of the induction length to the length of the reaction zone. By varying this parameter, the mechanisms of regular and irregular modes of instability and, finally, failure mode, were obtained. Ng and Lee [13], who used this three-step model for studying direct initiation of detonations, suggested that the ratio of induction and reaction zone lengths is the main parameter (independent of the rate process), which characterizes the stability of detonation waves.

A two-step reaction model was used by Sharpe [14] to study the linear stability of pathological detonations. In his model, the first step was exothermic and the second one was endothermic. He concluded that decreasing the value of $Ea_1 \quad Ea_2$ (the activation energy of the first step minus the activation energy of the second step) tends to destabilize pathological detonations.

Previous works indicated the important role of the induction and reaction lengths on instability. However, no attempt has been made to investigate this role systematically. For example, Howe et al. [15] showed that by changing the heat release rate, the induction delay has a destabilizing effect.

In this paper, a two-step reaction model is used. The first is a non-heat release induction step and the second is an exothermic reaction. In the next section, the model used for this investigation is presented and the modeling assumption behind it is described. Then, the spatial structure of the steady detonation wave admitted by the model is detailed and a description of how this structure changes, as Ea_1 and Ea_2 are varied, is presented. Furthermore, the numerical techniques used to obtain the numerical simulations of the nonlinear evolution of the pulsating, one-dimensional detonations are outlined and the results of this computational study are discussed. Finally, this paper ends with some conclusions that have been drawn from the investigation.

PHYSICAL MODEL

The detonation is initiated using a blast wave. The chemical reaction is modeled by two-step kinetics. The first step indicates an induction delay where no heat is released and reactant A is converted to an excited state, A^*. When the first reaction is near completion, the second step starts. In the second step, A^* is converted to B (product of reaction) and the energy of the reaction is released. These two steps are shown by two reactions:

$$A \rightarrow A^*, \quad \text{and} \quad A^* \rightarrow B. \tag{1}$$

The rates of reactions progress are given by:

$$w_1 = \frac{d\alpha}{dt} = \quad K_1 \alpha \exp\left(\frac{Ea_1}{RT}\right),$$

$$w_2 = \frac{d\beta}{dt} = \quad K_2 \beta \exp\left(\frac{Ea_2}{RT}\right), \tag{2}$$

where w_1 and w_2 are reaction rates, K_1 and K_2 are constant of reactions, T is the absolute temperature, R is the specific gas constant and Ea_1 and Ea_2 are activation energies. α and β are progress variables of two reactions. α, which represents consumption of reactants, decreases in the induction step from 1 to zero. (It is not possible to choose $\alpha = 0$, because the first step gives infinite time to be completed. Instead, the value of (10^{-5}) was chosen as a typical small value for α.) β, the progress variables of the second step,

remains constant during the induction step ($\beta = 1$) and decreases in exothermic step from 1 to zero.

The governing equations used are the one-dimensional reactive Euler equations:

$$\frac{\partial U}{\partial t} + \frac{\partial F}{\partial x} = s, \qquad U = \begin{bmatrix} \rho \\ \rho u \\ \rho e \\ \rho\alpha \\ \rho\beta \end{bmatrix},$$

$$F = \begin{bmatrix} \rho u \\ \rho u^2 + p \\ u(e+p) \\ \rho u\alpha \\ \rho u\beta \end{bmatrix}, \quad s = \begin{bmatrix} 0 \\ 0 \\ 0 \\ \rho w_1 \\ \rho w_2 \end{bmatrix}, \tag{3}$$

where variables ρ, u, p and e are density, particle velocity, pressure and total internal energy, respectively. A polytropic equation of state and an ideal thermal equation of state are used,

$$e = \frac{p}{\rho(\gamma \quad 1)} + \frac{u^2}{2} + Q\beta, \quad p = \rho RT, \tag{4}$$

where Q is the heat release per unit mass of the reactant and γ is the ratio of the specific heats. The dependent variables are non-dimensionalized with respect to the post shock steady-state properties of ZND detonation. Thus, the density, pressure and velocity are non-dimensionalized with the post shock density (ρ_s), pressure (γp_s) and sound speed (C_s), respectively. The characteristic length scale, L_c, is chosen arbitrarily as the half reaction length of the steady ZND detonation for $Ea_1 = 5$ and $Ea_2 = 28$. The characteristic time scale is $t_c = L_c/C_s$. Q, Ea_1 and Ea_2 are non-dimensionalized with RTo (for briefness, RTo will not be shown in the next sections). In all calculations here, $Q/RTo = 50$ and $\gamma = 1.2$ are used.

STEADY-STATE ZND STRUCTURE

For a set of known parameters (e.g., Q, Ea_1, Ea_2 and γ), detonation may be stable or unstable. Stability of detonation is determined with numerical simulation of unsteady gas-dynamic equations or linear stability calculations. Here, the first method is chosen.

The steady-state ZND structure of a detonation represents the structure of a stable detonation. The induction and reaction length of this structure are two meaningful length scales, which have been used by many researchers (e.g., [12,13]) to investigate the different detonation dynamic phenomena, such as the instability problem.

The steady-state ZND structure of detonation with two-step chemical kinetics can be determined by neglecting unsteady terms in the governing equations (Equations 2 to 4). The result is a set of linear differential equations with respect to X, which could be solved analytically. This solution is denoted in the following by the superscript*.

It is assumed that the steady detonation propagates with the CJ velocity to the left along the path $x^l = D^*_{CJ}t^l$ (superscript l denotes lab frame reference), where x^l denotes position of shock front and D^*_{CJ} is the CJ detonation velocity, which in terms of Q and γ is:

$$D^* = D^*_{CJ} = \left[\left(1+\frac{(\gamma^2 \quad 1)Q}{\gamma}\right)+\left(\left(1+\frac{(\gamma^2 \quad 1)Q}{\gamma}\right)^2 \quad 1\right)^{1/2}\right]^{1/2}. \tag{5}$$

Calculations are performed in a steady shock attached coordinate system (X):

$$X = x^l + D^*_{CJ}t^l. \tag{6}$$

Pressure, velocity and density (non-dimensionalized with shock conditions) can be shown to satisfy [6]:

$$p^* = a + (1 \quad a)(1 \quad bq^*)^{1/2},$$

$$u^* = \frac{(1 \quad p^*)}{\gamma M^*_s} + M^*_s,$$

$$\rho^* = \frac{M^*}{u^*}, \tag{7}$$

where:

$$M^{*2}_s = \frac{(\gamma \quad 1){D^*_{CJ}}^2 + 2}{2\gamma {D^*_{CJ}}^2 \quad (\gamma \quad 1)},$$

$$a = \frac{\gamma M^{*2}_s + 1}{(\gamma + 1)},$$

$$b = \frac{M^{*2}_s 2\gamma(\gamma \quad 1)}{(1 \quad a)^2(\gamma + 1)}. \tag{8}$$

M^*_s is the Mach number immediately behind the shock. The chemical energy release, q^*, in the steady wave satisfies:

$$q^* = \hat{Q}\beta^*, \tag{9}$$

where $\hat{Q} = Q/RT_s$ and the second reaction parameter, β^*, is assumed as an independent parameter in this step.

Note that the steady-state variables immediately behind the shock ($X = 0$), satisfy the shock conditions:

$$\rho^* = p^* = 1, \quad u^* = M_s, \quad \alpha^* = 1, \quad \beta^* = 1. \tag{10}$$

In the next step, X must be calculated from the following kinetics relations:

$$w_1^* = \frac{d\alpha}{dt} = u^*(\alpha)\frac{d\alpha}{dX} = \quad K_1\alpha^* \exp\left(\frac{\theta_1}{p^*v^*}\right),$$

$$w_2^* = \frac{d\beta}{dt} = u^*(\beta)\frac{d\beta}{dX} = \quad K_2\beta^* \exp\left(\frac{\theta_2}{p^*v^*}\right),$$

$$\theta_1 = Ea_1/(RT_s), \qquad \theta_2 = Ea_2/(RT_s). \tag{11}$$

It is assumed that $K_1 = K_2$. These two parameters are selected such that length scale becomes half reaction length for $Ea_1 = 5$ and $Ea_2 = 28$. Scaling procedure is further explained in Appendix A.

Since the second step starts after completion of the first step, it follows that:

$$X = \int_1^\alpha u^*(\alpha)/w_1^*(\alpha)d\alpha + \int_1^\beta u^*(\beta)/w_2^*(\beta)d\beta. \tag{12}$$

Because in the first step no heat is released, from Equation 7 it is observed that the pressure, velocity and density remain constant at their initial values and only α varies (see Figure 1). Thus, the length of the first step could be obtained from the following equation:

$$X = \int_1^\alpha M_s/w_1^*(\alpha)d\alpha = \frac{M_s\exp(\theta_1)}{K_1}\int_1^\alpha \frac{d\alpha}{\alpha}$$

$$= \frac{M_s\exp(\theta_1)}{K_1}\ln(\alpha). \tag{13}$$

The induction length, from the shock to the location where $\beta = 0.95$ (in which 5% of the heat of combustion is released) and the reaction length, from the end of the induction length to the location where $\beta = 0.05$ (in which 95% of the heat of combustion is released), are defined as shown in Figure 2. It is noted that the induction length is the sum of the first step length to the induction length associated with the second step.

It is interesting to study the changes in the steady wave structure as the activation energies of the two steps, Ea_1 and Ea_2, are varied.

Figure 3 shows the change in the steady wave structure for $Q = 50, \gamma = 1.2$ and $Ea_2 = 20$, while the activation energy of the first step (Ea_1) varies from 1 to 10. Across the shock, the pressure jumps abruptly to the Von Neumann state. During the induction period, the pressure remains constant. When energy starts to release in the reaction zone, the pressure drops. At the end of the reaction zone, the products are at

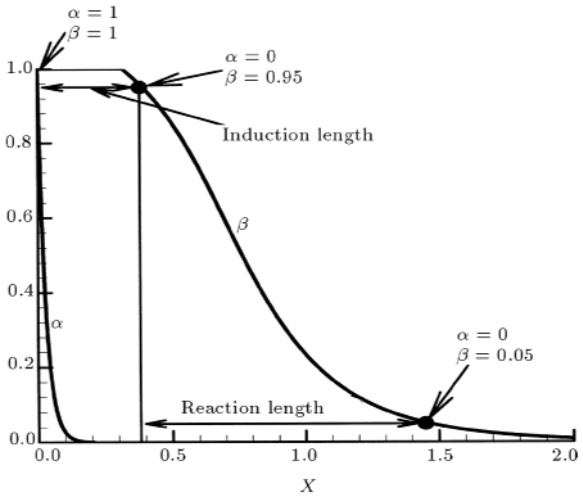

Figure 2. Definition of the induction and reaction lengths in terms of the second reaction parameter (β).

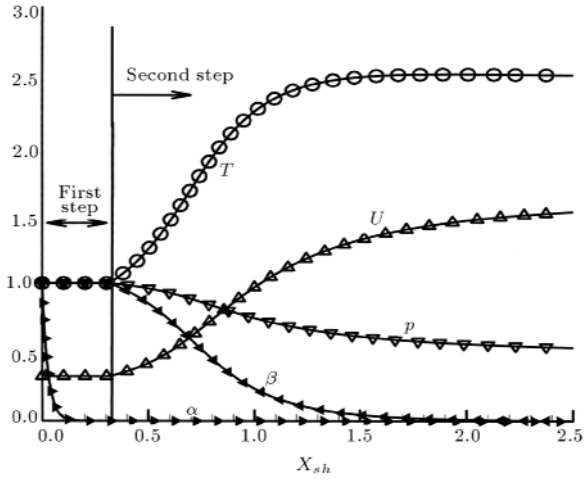

Figure 1. Steady ZND profiles for temperature (T), velocity (U), pressure (p), second reaction parameter (β) and first reaction parameter (α) ($Q = 50, \gamma = 1.2$, $Ea_2 = 25$ and $Ea_1 = 5$).

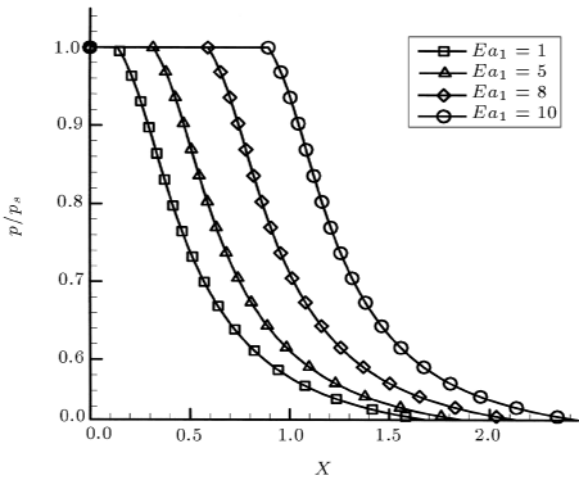

Figure 3. Steady ZND profiles: Pressure profile for increasing the activation energy of the first step ($Q = 50$, $\gamma = 1.2$ and $Ea_2 = 20$).

Table 1. Values of the induction length ($\Delta_{\text{induction}}$), the reaction length ($\Delta_{\text{reaction}}$) and the ratio of the reaction length to the induction length ($Q = 50$, $\gamma = 1.2$ and $Ea_2 = 20$).

Ea_1	$\Delta_{\text{induction}}$	Δ_{reaction}	$\Delta_{\text{reac.}}/\Delta_{\text{ind.}}$	Behavior
1.0	0.1651	0.6194	3.7528	Stable
5.0	0.3428	0.6194	1.8072	Unstable
8.0	0.6151	0.6194	1.0071	Unstable
10.0	0.9176	0.6194	0.6751	Unstable

equilibrium and the final state corresponds to the CJ condition. In Figure 3 it is seen that by increasing Ea_1, the induction length increases. The numerical values of the induction and the reaction lengths for Figure 3 are given in Table 1. It is seen that by increasing Ea_1, the induction length ($\Delta_{\text{induction}}$) increases, while the reaction length (Δ_{reaction}) remains constant (the same results were obtained with other definitions of reaction length) and, hence, the ratio of the reaction length to the induction length ($\Delta_{\text{reaction}}/\Delta_{\text{induction}}$) decreases. Since Ea_2 is constant, Ea_1 controls the induction length.

Figure 4 shows the change in the steady wave structure for $Q = 50, \gamma = 1.2$ and $Ea_1 = 5$, while the activation energy of the second step varies. For $Ea_2 = 10$, the structure of steady detonation is very close to the square wave model [6]. For a higher value of Ea_2, the difference between the structure of steady detonation wave and this model becomes greater. Table 2 shows the induction and reaction lengths for different Ea_2. By increasing Ea_2, the induction length increases slightly. This is due to increasing the induction length associated with the second step. For $Ea_2 > 35$, the induction length of the second step is greater than the induction length of

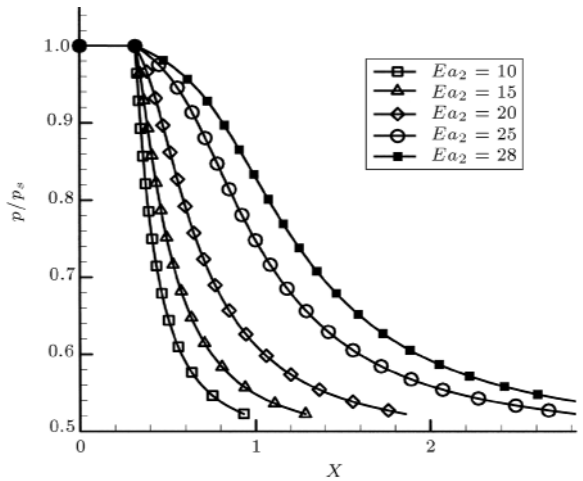

Figure 4. Steady ZND profiles: Pressure profile for increasing the activation energy of the second step ($Q = 50, \gamma = 1.2$ and $Ea_1 = 5$).

Table 2. Values of the induction length ($\Delta_{\text{induction}}$), the reaction length ($\Delta_{\text{reaction}}$) and the ratio of the reaction length to the induction length ($Q = 50, \gamma = 1.2$ and $Ea_1 = 5$).

Ea_2	$\Delta_{\text{induction}}$	Δ_{reaction}	$\Delta_{\text{reac.}}/\Delta_{\text{ind.}}$	Behavior
10.0	0.3186	0.2198	0.6899	Unstable
15.0	0.3251	0.3659	1.1253	Unstable
20.0	0.3428	0.6194	1.8072	Unstable
22.0	0.3565	0.7690	2.1572	Stable
25.0	0.3906	1.0709	2.7414	Stable
28.0	0.4529	1.5050	3.3229	Unstable
35.0	0.8747	3.4655	3.9617	—*
37.5	1.2382	4.7385	3.8270	—*
50.0	11.601	25.764	2.2208	—*

* Although this case was not simulated numerically, as noted in the introduction, the instability of this case is obvious.

the first step, thus, Ea_2 controls the induction length. The reaction length (Δ_{reaction}) increases, when Ea_2 increases. The ratio of reaction length to induction length ($\Delta_{\text{reaction}}/\Delta_{\text{induction}}$) increases for $Ea_2 < 35$ and, then, decreases for $Ea_2 > 35$. It is seen that by increasing Ea_2, both induction and reaction lengths increase. However, for small values of Ea_2 (i.e., $Ea_2 < 25$), the induction length of the second step is small relative to the reaction length and the total induction length. Therefore, the induction length approximately remains constant. Above this limit, the induction length of the second step becomes significant and Ea_2 controls both the induction and reaction lengths. Decreasing of the ratio ($\Delta_{\text{reaction}}/\Delta_{\text{induction}}$) for $Ea_2 > 35$ is due to the dominant effect of the second step. At the limit, when Ea_2 is very large relative to Ea_1, the two-step model is similar to the one-step model. Therefore, it can be concluded that small values of Ea_2 control the reaction length and large values of Ea_2 control both induction and reaction lengths. Furthermore, this analysis shows the salient features of the two-step model in order to study the individual effects of induction and reaction lengths.

The variation of the ratio of reaction length to the induction length with Ea_2 is drawn in Figure 5. This ratio has been introduced by many investigators as a criterion, which controls the stability of gaseous detonation, (e.g., [13,15]). For a one-step model, the ratio is decreased by increasing the activation energy. Therefore, for a single-step model, decreasing the ratio causes the instability. Ng et al. [13] obtained the same conclusion for a three-step model. However, the present analysis of the ZND structure for a two-step model predicts that the variation of the ratio with the activation energy of the second step has an extremum (Figure 5). This means that for $Ea_2 < 35$, the ratio

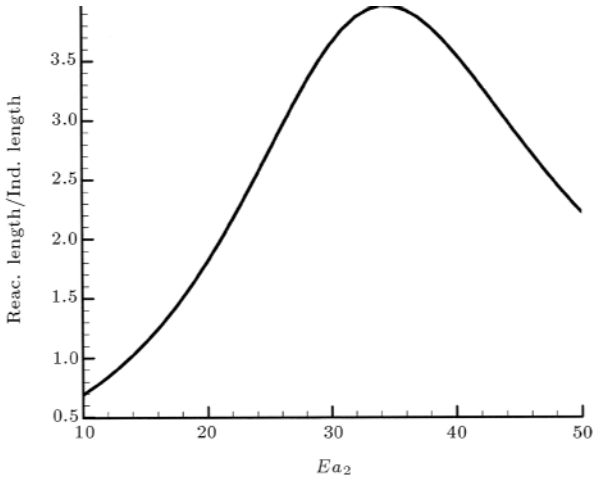

Figure 5. Variation of the ratio of the reaction length to the induction length vs Ea_2.

increases with increasing Ea_2 while, for $Ea_2 > 35$, the ratio decreases with increasing Ea_2. To study the stability behavior of the two-step model, the complete unsteady gas dynamics equations should be solved. This is the subject of the next section.

NUMERICAL METHOD

Over the past 40 years, a great number of numerical schemes have been devised for the simulation of gas dynamics. In recent years, a number of new shock-capturing schemes, often called high-resolution schemes, have been proposed. Among them are the FCT, MUSCL, ENO and PPM methods. There are several excellent review articles, which compare these schemes from different points of view. Interested readers should refer to those articles, particularly the paper of Yang et al. [16] and the Ph.D. thesis of Bourlioux [17]. After comparing different schemes, the PPM (Piecewise Parabolic Method) [18] is recommended as the best in overall performance. Therefore, in the present work, PPM is chosen as the main gasdynamics solver. Details of this method are explained in Appendix B.

In analyzing the propagation of pulsating detonation, the tracking of the shock front plays an essential role. In the past twenty years, several methods have been developed to track the front and other discontinuities in the flow field. For the purpose of this paper, the simplest one is the conservative front tracking of Chern and Colella [19], which has been utilized in the present study. Since all reactions are completed in a narrow region close to the shock, it is more economical to use a fine grid only in this region and coarse grid elsewhere. To fulfill this requirement, a simple version of the "Adaptive Mesh Refinement" of Berger and Collela [20] has been used. The entire domain is covered by coarse grids and the fine meshes are superimposed on the coarse grid near the front. The number of meshes that are necessary, depends on the behavior of the shock front [12]. Unless noted otherwise, the computations were performed using a grid resolution of 20 points in the half-reaction length ($L_{1/2}$) as the fine grid. It was observed that further increases in grid resolution have no effect other than to cause very small changes in the amplitude and period of the shock pressure oscillation. For some cases up to 120 points per half reaction length were used. The developed code is validated via several test problems [21].

RESULTS AND DISCUSSION

Previous researches have shown that for a one-step Arrhenius kinetics model, the activation energy is the main parameter, which determines the instability of CJ detonation (e.g., [5,6]). In a one-step model, for a mixture with $Q = 50$ and $\gamma = 1.2$, the ZND structure is unstable for Ea higher than 25 [6]. Increasing the activation energy beyond this limit causes the detonation front to exhibit oscillatory behavior as shown in Figure 6. In this figure the shock pressure, normalized with ZND shock pressure, is used for demonstrating detonation front behavior. Therefore, increasing Ea in the one-step model destabilizes a detonation.

The effect of the activation energies of the two-step model on detonation front behavior has been studied in this work. Calculations were arranged in two stages. At each stage, one of the activation energies was kept constant and the other was changed. From these results, the front shock pressure is plotted vs the instantaneous shock location.

At the first stage, the activation energy of the second step was kept constant (i.e., $Ea_2 = 20$) and Ea_1 was changed. The variation of shock pressure for

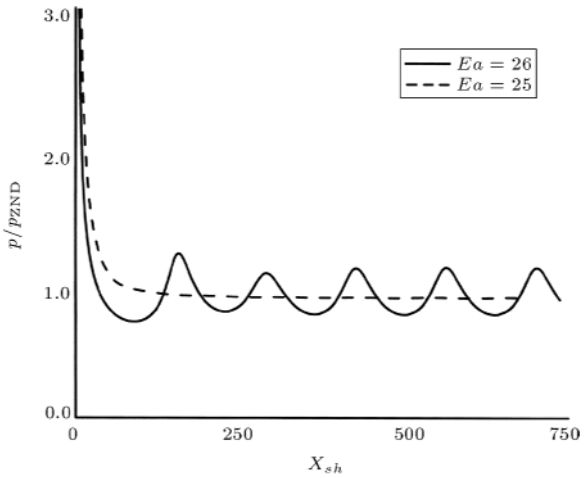

Figure 6. Effect of the activation energy of the one-step model on detonation instability.

$Ea_1 = 5$ is demonstrated in Figure 7. It is seen that the front shows regular oscillation, with small amplitude. Increasing Ea_1 to 8 causes larger amplitude to occur (Figure 8). An irregular oscillation appears as the activation energy increases to 10 (Figure 9). In this case, it is observed that increasing the activation energy of the induction step promotes detonation instability. This result is similar to that of the one-step model.

Table 1 shows induction and reaction lengths and the stability status of these cases. It is observed that increasing induction length (occurred by increasing Ea_1) destabilizes detonation. The reaction length remains constant because Ea_2 is kept constant. Thus, decreasing the ratio of reaction length to induction length, as a criterion, causes instability of detonation.

In the second stage of the calculations, the effect of Ea_2 on detonation instability has been studied while Ea_1 was kept constant (i.e., $Ea_1 = 5$). Figure 10 shows the variation of the front shock pressure for

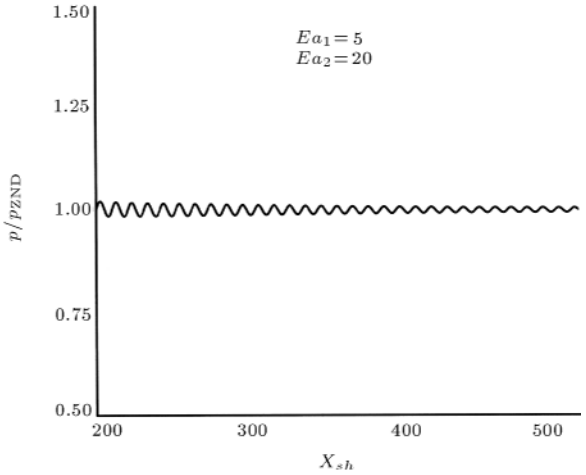

Figure 7. Regular oscillation with small amplitude of the detonation shock pressure for $Ea_1 = 5$.

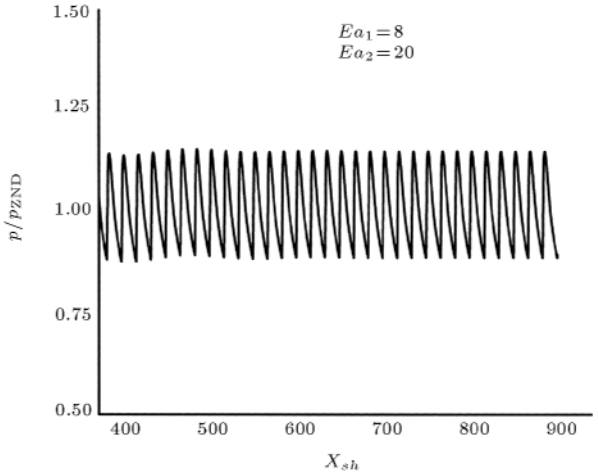

Figure 8. Regular oscillation with large amplitude of the detonation shock pressure for $Ea_1 = 8$.

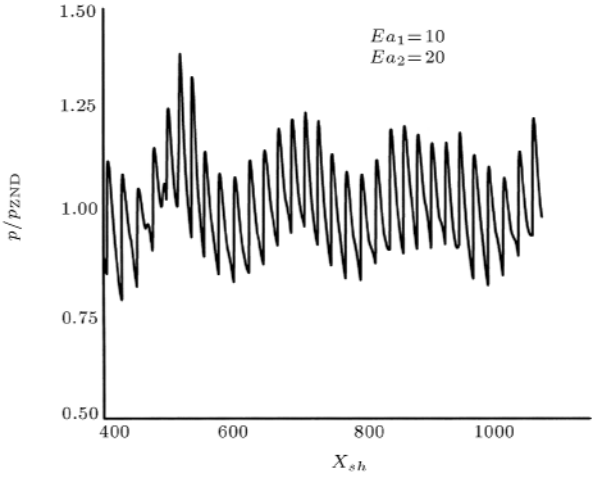

Figure 9. Irregular oscillation with large amplitude of the detonation shock pressure for $Ea_1 = 10$.

$Ea_2 = 15$. An almost regular oscillation with large amplitude is observed (it is noted that the steady structure of this case is similar to the square wave model, Figure 4). Increasing Ea_2 to 20 causes a smaller amplitude oscillation with respect to $Ea_2 = 15$ (Figure 11). As Figure 12 shows, further increasing Ea_2 to 22 stabilizes the front propagation. The front is also stable for $Ea_2 = 23$ to 25. Figure 13 shows the detonation front behavior for $Ea_2 = 28$. An oscillatory variation of the front pressure with a very large period (in comparison with other cases) is observed for this case. Therefore, it is concluded that increasing the activation energy of the exothermic step decreases the amplitude of oscillation for $Ea_2 < 22$, while increasing the amplitude for $Ea_2 > 25$.

Table 2 shows induction and reaction lengths and the stability status of the above cases. It is observed that by increasing the reaction length and the ratio of the reaction length to the induction length (both occurred by increasing Ea_2), detonation tends to be

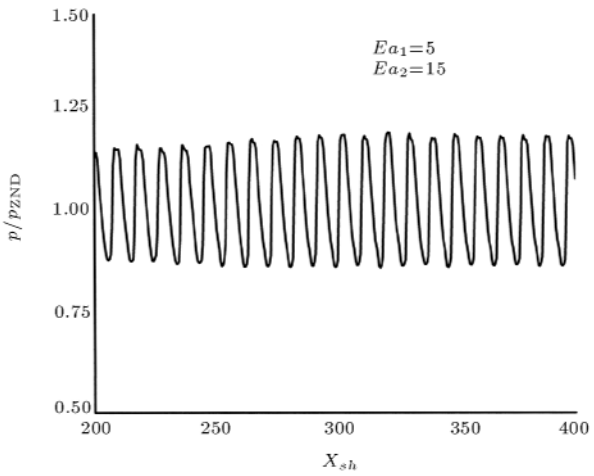

Figure 10. Regular oscillation with large amplitude of the detonation shock pressure for $Ea_2 = 15$.

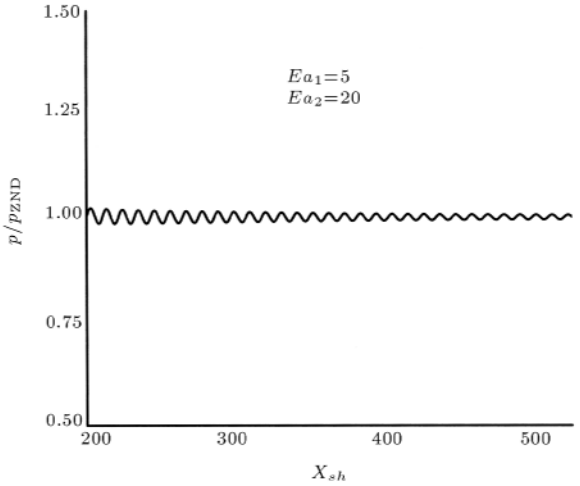

Figure 11. Regular oscillation with small amplitude of the detonation shock pressure for $Ea_2 = 20$.

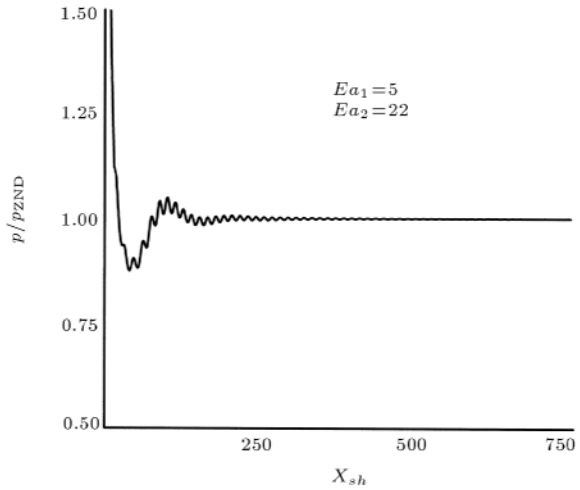

Figure 12. Stable behavior of the detonation shock pressure for $Ea_2 = 22$.

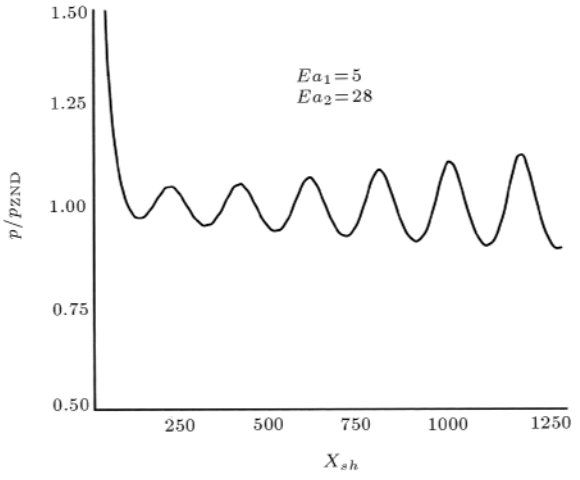

Figure 13. Oscillatory variation of the detonation shock pressure for $Ea_2 = 28$.

stabilized for $Ea_2 < 22$. However, for $Ea_2 > 25$, detonation becomes more unstable. The behavior of the induction and reaction lengths does not change during increasing Ea_2. From Figure 5 it is seen that by increasing Ea_2, the ratio of reaction length to induction length increases for $Ea_2 < 35$ and decreases for $Ea_2 > 35$. As expected, the behavior of this ratio is changed when detonation is stabilized and then destabilized. However, the change in the behavior of the ratio of the ZND structure does not coincide with the change in the stability status of detonation determined by numerical simulation.

CONCLUSION

Detonation instability (using a two-step chemical kinetics model) has been studied in this work. It was shown that:

1. For a fixed Ea_2, increasing Ea_1 (i.e., the activation energy of the induction step) increases the induction length and destabilizes detonation, the same behavior as the one-step model;
2. For a fixed $Ea_1 = 5$, increasing Ea_2 (i.e., the activation energy of the heat release step) increases the reaction length and the induction length. Increasing the reaction length may have a dominant stabilizing effect for $Ea_2 < 22$;
3. For a fixed $Ea_1 = 5$, if Ea_2 increases above 25, increasing the induction length has a dominant destabilizing effect;
4. The ratio of reaction length to induction length of the ZND detonation characterizes detonation instability, but its behavior does not exactly coincide with the instability status of detonation, which is determined by the numerical solution of the unsteady governing equations.

REFERENCES

1. Fickett, W. and Davis, W.C., *Detonation*, University of California Press, CA, USA (1979).
2. Strehlow, R.A., *Combustion Fundamentals*, McGraw-Hill (1997).
3. Alpert, R.L. and Toong, T.Y. "Periodicity in exothermic hypersonic flows about blunt projectiles", *Acta Astron.*, **17**, pp 538-560 (1972).
4. Kaneshige, M.J. and Shepherd, J.E. "Oblique detonation stabilized on a hypervelocity projectile", *26th Symposium (Intern.) on Combustion*, The Combustion Institute, p 3015 (1996).
5. Erpenbeck, J.J. "Stability of idealized one-reaction detonations", *Phys. Fluids*, **5**, pp 604-614 (1962).
6. Lee, H.I. and Stewart, D.S. "Calculation of linear detonation stability: One dimensional instability of

plane detonation", *J. Fluid Mech.*, **216**, pp 103-132 (1990).

7. Buckmaster, J.D. and Ludford, G.S.S. "The effect of structure on the stability of detonations I. Role of the induction zone", *Proc. 21th Symp. on Combustion*, pp 1669-1675 (1986).
8. Sharpe, G.J. "Linear stability of idealized detonations", *Proc. R. Soc. Lond.*, **453**, pp 2603-2625 (1997).
9. Fickett, W. and Wood, W.W. "Flow calculation for pulsating one-dimensional detonations", *Phys. Fluids*, **9**, pp 903-916 (1966)
10. Abouseif, G. and Toong, T.Y. "Theory of unstable one-dimensional detonations", *Combustion & Flame*, **45**, pp 64-94 (1982).
11. Bourlioux, A., Majda, A. and Roytburd, V. "Theoretical and numerical structure for unstable one-dimensional detonations", *SIAM J. Appl. Math*, **51**, pp 303-343 (1991).
12. Short, M. and Quirk, J.J. "On the nonlinear stability and detonability of a detonation wave for a model three-step chain-branching reaction", *J. Fluid Mech.*, **339**, pp 89-119 (1997).
13. Ng, H.D. and Lee, J.H.S. "Direct initiation of detonations with multi-step reaction scheme", Under consideration for publication in *Journal of Fluid Mechanics* (2001).
14. Sharpe, G.J. "Linear stability of pathological detonations", *J. Fluid Mech.*, **401**, pp 311-338 (1999).
15. Howe, P., Frey, R. and Melani, G. "Observation concerning transverse waves in solid explosives", *Combustion Science and Technology*, **14**, pp 63-74 (1976).
16. Yang, H.Q. and Przekwas, A.J. "A comparative study of advanced shock-capturing schemes applied to Burger's equation", *J. Comput. Phys.*, **102**, pp 139-159 (1992).
17. Bourlioux, A. "Numerical studies of unstable detonations", Ph.D. Thesis, Department of Applied and Computational Mathematics, Princeton University, USA (1991).
18. Colella, P. and Woodward, P.R. "The piecewise parabolic method (PPM) for gas-dynamical simulations", *J. Comput. Phys.*, **54**, pp 174-201 (1984).
19. Chern, I.L. and Colella, P., *A Conservative Front Tracking Method for Hyperbolic Conservation Laws*, Lawrence Livermore National Laboratory, UCRL 97200 (1987).
20. Berger, M.J. and Colella, P. "Local adaptive mesh refinement for shock hydrodynamics", *J. Comput. Phys.*, **82**, pp 64-84 (1989).
21. Mazaheri, K. "Mechanism of the onset of detonation in direct initiation", Ph.D. Thesis, Department of Mechanical Engineering, McGill University, Canada (1997).

APPENDIX A

Scaling Procedure

The half reaction length of the case ($Ea_1 = 5$ and $Ea_2 = 28$) is chosen as length scale. This length can be calculated from Equation 12.

$$l_c = 1 = X_\alpha + \int_1^{\frac{1}{2}} u^*(\beta)/w_2^*(\beta)d\beta$$

$$= \frac{11.513 M_s \exp(\theta_1)}{K_1} + \int_1^{\frac{1}{2}} u^*(\beta)/w_2^*(\beta)d\beta. \qquad \text{(A1)}$$

If $Q = 50$ and $\gamma = 1.2$ then:

$$M_s = 0.324, \quad \theta_1 = 1.039, \quad \theta_2 = 5.817. \qquad \text{(A2)}$$

Calculating Equation A1 gives $K_1 = K_2 = 33.45$.

APPENDIX B

Piecewise Parabolic Method (PPM)

The Piecewise Parabolic Method (PPM) of Colella and Woodward [18] is a higher-order extension of the Godunov method. To explain PPM, the numerical solution of an initial-boundary value problem is considered for the hyperbolic equation:

$$u_t + \alpha f_x = 0, \qquad \text{(B1)}$$

here, $u(x,t)$ is an unknown function of x and t and $f(u)$ is called the flux function. Figure B1 illustrates space-time domain and indexing.

Equation B1 has the following discretized form:

$$u_j^{n+1} = u_j^n \quad \frac{\alpha \Delta t}{\Delta x}(f_{j+\frac{1}{2}} \quad f_{j\ \frac{1}{2}}), \qquad \text{(B2)}$$

where $\Delta x = x_{j+1/2} \quad x_{j\ 1/2}$ and $\Delta t = t^{n+1} \quad t^n$. "$f$" is the flux at the interface between two cells. Knowing the value of u at time level t^n, the key to finding the solution at a new time level, t^{n+1}, is

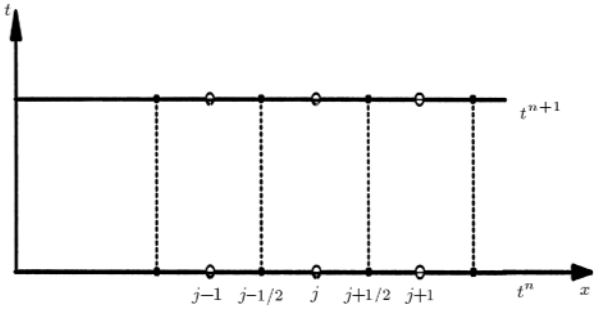

Figure B1. Computational domain, indexing.

to properly compute the interface fluxes, $f_{j+1/2}$ and $f_{j\ 1/2}$. Indeed, the difference between the different methods mentioned above is in the treatment of these fluxes.

The main contribution of Godunov is the way in which the fluxes are computed. Instead of using some averaging between cell values, in the Godunov method the fluxes are computed from an exact solution of the Riemann problem at the interface between two adjacent cells. PPM is a higher-order Godunov method which, instead of using a constant value for the dependent variable at each cell (as in the Godunov method), uses a parabolic profile in each cell with form:

$$u(x) = u_{j\ \frac{1}{2}} + \xi[\Delta u_j + u_{6,j}(1 \quad \xi)], \tag{B3}$$

where:

$$\xi = \frac{(x \quad x_j)}{\Delta x}, \quad x_{j\ \frac{1}{2}} \le x \le x_{j+\frac{1}{2}}, \tag{B4}$$

$$\Delta u_j = u_{j+\frac{1}{2},L} \quad u_{j\ \frac{1}{2},R}, \tag{B5}$$

$$u_{6,j} = 6[u_{j\ \frac{1}{2}} (u_{j+\frac{1}{2},L} + u_{j\ \frac{1}{2},R})]. \tag{B6}$$

The left and right side state variables for the Riemann solver, $u_{j+1/2,L}$ and $u_{j+1/2,R}$, are calculated by first using an interpolation scheme to obtain $u(x)$ and then, an approximation to the value of u at $x_{j+1/2}$, subject to the constraint that $u_{j+1/2}$ does not fall outside of the range of values given by u_j and u_{j+1}. The interface value is calculated as:

$$u_{j+\frac{1}{2}} = \frac{1}{2}(u_{j+1} + u_j) + \frac{1}{6}(\delta_l u_j \quad \delta_l u_{j+1}), \tag{B7}$$

where:

$$\delta_l u_j = \min \ |\delta u_j|, 2|\Delta_{j+1/2}|, 2|\Delta_{j\ 1/2}|) \ \mathrm{sign}(\delta u_j),$$

$$\text{if}: \ \Delta_{j+1/2}.\Delta_{j\ 1/2} > 0, \tag{B8}$$

$$\delta_l u_j = 0, \ \text{otherwise}. \tag{B9}$$

Here, $\delta u_j = \frac{1}{2}(u_{j+1} \quad u_{j\ 1}), \Delta_{j+1/2} = u^n_{j+1} \quad u^n_j$ and $\Delta_{j\ 1/2} = u^n_j \quad u^n_{j\ 1}$.

In smooth regions away from the high gradients, the left and right states can be computed directly as:

$$u_{j+\frac{1}{2},L} = u_{j+\frac{1}{2},R} = u_{j+\frac{1}{2}}, \tag{B10}$$

then, the interpolation function is continuous at the interface. If the interpolation function, $u(x)$, takes on the values, which are not between $u_{j+1/2,L}$ and $u_{j+1/2,R}$, to satisfy the monotonocity condition, more limitations must be applied. The left and right states, $u_{j+1/2,L}$ and $u_{j+1/2,R}$, are modified so that $u(x)$ is a monotone function on each cell. The new expressions for $u_{j+1/2,L}$ and $u_{j+1/2,R}$ are as follows:

I) $u_{L,j} = u_{R,j} = u^n_j$,

if: $(u_{R,j} \quad u^n_j)(u^n_j \quad u_{L,j}) \le 0$,

II) $u_{L,j} = 3u^n_j \quad 2u_{R,j}$,

if: $(u_{R,j} \quad u_{L,j}) \left[u^n_j \quad \frac{1}{2}(u_{R,j} + u_{L,j})\right] > \frac{(u_{R,j} \quad u_{L,j})^2}{6}$,

III) $u_{R,j} = 3u^n_j \quad 2u_{L,j}$,

if: $\frac{(u_{R,j} \quad u_{L,j})^2}{6} > (u_{R,j} \quad u_{L,j}) \left[u^n_j \quad \frac{1}{2}(u_{R,j} + u_{L,j})\right]$. (B11)

Finally, the cells interface flux is computed as:

$$f_{j+\frac{1}{2},L}(y) = u_{R,j} \quad \frac{x}{2}\left[\Delta u_j \quad (1 \quad \frac{2}{3}x)u_{6,j}\right],$$

$$\text{where: } x = \frac{y}{\Delta\xi_j},$$

$$f_{j+\frac{1}{2},R}(y) = u_{L,j+1} \quad \frac{x}{2}\left[\Delta u_{j+1} + (1 \quad \frac{2}{3}x)u_{6,j+1}\right],$$

$$\text{where: } x = \frac{y}{\Delta\xi_{j+1}}. \tag{B12}$$

In Equations B11 and B12, $y = \alpha\Delta t$ if $\alpha > 0$ and $y = \ \alpha\Delta t$ if $\alpha < 0$.

With the left and right states at the interface known, the next step is to solve the Riemann problem to compute the value of the state variables at the interface. Details of the PPM method for the system of Euler equations are described by Colella et al. [18].